ISSN 0021-3640, JETP Letters, 2023, Vol. 117, No. 12, pp. 932–937. © Pleiades Publishing, Inc., 2023.
Russian Text © The Author(s), 2023, published in Pis'ma v Zhurnal Eksperimental'noi i Teoreticheskoi Fiziki, 2023, Vol. 117, No. 12, pp. 929–934.

CONDENSED MATTER

Dependence of the Relaxation Rate of Coherent States on the Number of Correlated Spins and the Order of Coherence

V. E. Zobov[a] and A. A. Lundin[b,*,]**

[a] *Kirensky Institute of Physics, Federal Research Center KSC, Siberian Branch, Russian Academy of Sciences, Krasnoyarsk, 660036 Russia*

[b] *Semenov Institute of Chemical Physics, Russian Academy of Sciences, Moscow, 117977 Russia*

** e-mail: rsa@iph.krasn.ru*

*** e-mail: ya-andylun2012@yandex.ru*

Received March 28, 2023; revised May 17, 2023; accepted May 18, 2023

The relaxation of the components of the multiple-quantum NMR spectrum of a solid under the effect of the dipole–dipole interactions during the evolution period is considered. It is taken into account that clusters of dynamically correlated spins of different sizes are formed in the preparatory period, and their degradation depends on their size and coherence order. To calculate the size distribution function of clusters and their degradation function, a physical model including relaxation processes is developed. Using this model, an analytical result for a multiple-quantum spectrum is obtained. Agreement is obtained between the theoretical and experimental dependences of the coherence degradation rates in adamantane scaled by the square root of the average cluster size. The parameters of the above functions are found from the comparison of these dependences.

DOI: 10.1134/S0021364023601525

The emergence and growth of dynamic correlations between particles and their relaxation caused by various degradation mechanisms play a fundamental role in many-body physics. Previously, this kind of research was carried out in order to develop nonequilibrium statistical mechanics [1]. However, at present, their study has become necessary for the practical implementation of quantum devices and technologies [2–4], including the design and usage of the so-called noisy intermediate-scale quantum computers [5, 6], the size of which is limited by decoherence processes. For example, in [7], a noisy intermediate-scale quantum computer was implemented using dynamically correlated spins of ^{1}H nuclei in polycrystalline adamantane. The spin system is controlled by nuclear magnetic resonance (NMR) methods using a sequence of coherent radio-frequency pulses. Under the experimental conditions, the achieved register size was 25 spins.

Multiple-quantum NMR spectroscopy of solids stands out among the methods for studying multiparticle dynamical correlations [8, 9]. In multiple-quantum experiments, by irradiating a spin system with a sequence of coherent radio-frequency pulses, researchers convert the Hamiltonian of internuclear spin–spin interactions (usually the dipole–dipole interaction) into a "preplanned" internuclear spin–spin Hamiltonian called the effective Hamiltonian. Then, using it, one observes the development of multispin correlations (among several thousand spins) [10–13] and controls the growth of these correlations and their degradation [8, 14–16]. Despite a large number of published works, there are still many unsolved problems in this field [15, 16]. One of the central (but also most difficult) problems in the field of multiple-quantum spin dynamics is the description of the degradation of large multiple-quantum clusters depending on the size and quantum number (coherence order).

In pioneering work [10], the relaxation of the components of the multiple-quantum spectrum in polycrystalline adamantine was measured at an increase in the duration of the interval of the evolution with a dipole–dipole interaction Hamiltonian between the preparatory period and the mixing period. The dependence of the decoherence rate on the coherence order and on the size of the average cluster of dynamically correlated spins, which is formed as a result of two-quantum-two-spin interaction in the preparatory period and is determined by its duration, is revealed.

The first theoretical analysis of these results was given in [17]. The authors proposed to divide the field from the dipole–dipole interaction among cluster spins into correlated and uncorrelated parts. Proceeding from this, the signal from the multiple-quantum component of the spectrum is represented as the sum

of two terms from the spins, the dynamics of which is determined by the correlated and uncorrelated fields. The first term is a function of the coherence order, and the second term is a function of the number of spins in the cluster. The degree of correlation is determined by the ratio of the amplitudes of the two terms.

Although the theoretical dependences are similar to the experimental results, the assumed heterophase nature of the complex desired time correlation function needs to be substantiated in the homogeneous spin system of adamantane under consideration at high temperatures. The assumption that the local field consists of two parts on each spin rather than on different spins is more natural and has long been used to explain the dynamics of the nuclear spin system of a solid body. For example, the division of the local field on any selected spin into two components, from the nearest neighbors (cells) and from more distant spins (far environment), made it possible to explain the characteristic features of the free precession signal (Fourier transform of the NMR absorption spectrum) in a solid [18] and to correctly describe them for the first time.

Dividing the local field of the dipole–dipole interaction on each of the spins of the cluster of dynamically correlated spins into two components [19], we obtained a function describing the degradation of the cluster in the form of a product of two factors from two contributions to the local field:

$$\Gamma_{KM}(t_1) = \exp(-KB^2t_1^2/2)\exp(-A^2M^2t_1^2), \qquad (1)$$

where t_1 is the duration of the evolution interval, K is the number of spins in a cluster, M is the coherence order, B^2 is the parameter characterizing the uncorrelated contribution to the local field on each of the cluster spins independent of the local field on other spins, and A^2 is the parameter characterizing the field averaged over the cluster, which acts on all spins of the cluster in a correlated manner. The order of magnitude of the parameters B^2 and A^2 is determined by the second moment of the spectrum of the autocorrelation function of one spin m_2, but their exact calculation is almost impossible [19]. Therefore, we assume them further as some phenomenological constants determined from experimental data. Using representation (1), we analyzed in [19] experimental dependences from [10, 11]. Since the experimental error increases rapidly with M (see Fig. 5 in [10]), approaching 100% at large M values, and the presented curves have an unusual shape, we used only the central part of experimental results when processing the experiment to extract data [19].

In the formulas obtained in the theoretical approaches described above, the cluster degradation rate on the coherence order M appears only in the contribution from the correlated field, while the contribution from uncorrelated fields on the cluster spins is independent of M but depends only on the number of spins in the cluster. The reason is that degradation over the evolutionary period under the action of the dipole–dipole interaction of a single cluster of correlated spins of the average size $\bar{K}$ formed during the preparatory period is considered in both theories. In fact, the density matrix at the end of the preparatory period is the sum of contributions from clusters of different sizes K, each degrading at its own rate during the evolutionary period.

In this work, we calculate the M dependence of the decoherence rate of the components of the multiple-quantum spectrum, taking into account the formation of clusters of different sizes during the preparatory period. To set the weights for clusters of different sizes, we use the distribution function proposed in our works [20–24] within a simple model that corresponds to experiment and leads to an exponential increase in the average size of a cluster of correlated spins with the duration of the preparatory period.

Now we represent the observed multiple-quantum spectrum $G_M(T,t_1)$ as the following sum of multiple-quantum spectra g_{KM} of clusters of different sizes K formed in the preparatory period of the duration T and degraded then during the evolutionary period of the duration t_1:

$$G_M(T,t_1) = \sum_{K=|M|}^{\infty} g_{KM}\Gamma_{KM}(t_1)P(K,T), \qquad (2)$$

where $\Gamma_{KM}(t_1)$ is the degradation function (1) and $P(K,T)$ is the distribution over the number of clusters with K spins. Following the combinatorial theory [8], the multiple-quantum spectrum of an individual cluster is described by the Gaussian function

$$g_{KM} = \frac{1}{\sqrt{\pi K}}\exp\left(-\frac{M^2}{K}\right). \qquad (3)$$

The size distribution function of clusters is taken in the form

$$P(K,T) = \frac{(\tanh^2(T/\sqrt{2}))^{K-1}K}{\cosh^4(T/\sqrt{2})}, \qquad (4)$$

which is obtained in [22–24] within a simple cluster growth model and satisfies the normalization condition $\sum_{K=1}^{\infty} P(K,T) = 1$. The corresponding average cluster size

$$\bar{K}_0(T) = \sum_{K=1}^{\infty} KP(K,T) = 1 + 2\sinh^2(T/\sqrt{2}) \qquad (5)$$

increases exponentially with T as $\bar{K}_0(T) \sim \exp(\sqrt{2}T)/2$ (at $T \gg 1$), which is characteristic of dense spin systems such as adamantane or fluorite [20, 21]. (Here and below, the time is expressed in units of the inverse

second moment ($1/\sqrt{m_2}$) of the autocorrelation function.)

It is quite obvious that the main contribution to the multiple-quantum spectrum determined by the sum (2) at large times T comes from large clusters ($K \gg 1$). Using Eq. (5), which makes it possible to express hyperbolic functions in Eq. (4) in terms of $\bar{K}_0(T)$, the formulas for transforming hyperbolic functions, and the second remarkable limit, it is easy to obtain for large K values

$$P(K,T) = K\left(\frac{2}{\bar{K}_0+1}\right)^2\left(\frac{\bar{K}_0-1}{\bar{K}_0+1}\right)^{K-1}$$
$$\approx K\left(\frac{2}{\bar{K}_0+1}\right)^2\exp\left(-2\frac{K-1}{\bar{K}_0+1}\right) \quad (6)$$
$$\sim K\left(\frac{2}{\bar{K}_0}\right)^2\exp\left(-2\frac{K}{\bar{K}_0}\right).$$

Substituting Eqs. (1) and (6) into Eq. (2), replacing summation by integration with a zero lower limit, which is true at least for large clusters, and taking the contribution from the correlated field out of the integrand, we calculate the integral [25]

$$G_M(T,t_1) = \exp(-A^2M^2t_1^2)\left(\frac{2}{\bar{K}_0}\right)^2$$
$$\times\int_0^\infty \exp\left\{-K\frac{2}{\bar{K}_0}(1+\bar{K}_0B^2t_1^2/4) - \frac{M^2}{K}\right\}\sqrt{K/\pi}dK \quad (7)$$
$$= \frac{1}{2(q)^{3/2}}\left(1+2|M|\sqrt{q}\right)\exp\left(-2|M|\sqrt{q}\right)\exp(-A^2M^2t_1^2).$$

Here, $q = (2/\bar{K}_0)(1+\bar{K}_0B^2t_1^2/4)$.

Because of degradation, the total intensity of the multiple-quantum spectrum

$$N(T,t_1) = \int_{-\infty}^{\infty} G_M(T,t_1)dM \quad (8)$$

decreases with increasing t_1. The shape of the multiple-quantum spectrum is described by the function obtained from Eq. (7) after normalization to $N(T,t_1)$. In particular, without the correlated contribution to the local field (i.e., at $A = 0$), we obtain the universal form of the multiple-quantum spectrum

$$f_1(M) = G_M(T,t_1)/N(T,t_1)$$
$$= \frac{1}{\sqrt{2\bar{K}_1}}\left(1+2\sqrt{\frac{2M^2}{\bar{K}_1}}\right)\exp\left(-2\sqrt{\frac{2M^2}{\bar{K}_1}}\right), \quad (9)$$

scalable to the average cluster size of correlated spins,

$$\bar{K}_1 = 2\langle M^2\rangle = \bar{K}_0/(1+\bar{K}_0B^2t_1^2/4), \quad (10)$$

obtained with allowance for degradation only from the independent contribution to the local field and equal to twice the second moment of the multiple-quantum spectrum. Although the ratio of the average cluster size to the second moment of the spectrum $\langle M^2\rangle$ is the same as that for the Gaussian function given by Eq. (3), the spectrum shape given by Eq. (9) differs significantly from the Gaussian one. The resulting dependence of the spectrum on M is exponential in M in contrast to the Gaussian dependence exponential in M^2. In addition, the found spectrum decreases by a factor of e at $M_e \approx 1.05\sqrt{\langle M^2\rangle}$, while such a decrease for the Gaussian function occurs at $M_e = \sqrt{2\langle M^2\rangle}$. Thus, the model developed in this work made it possible to explain the exponential shape of the multiple-quantum spectra observed in experiments [14, 26].

Expression (7) obtained for the multiple-quantum spectrum allows one to calculate the relaxation rate of the spectral component with the coherence order M determined in terms of time $\tau = t_1$, at which its amplitude decreases by a factor of e. This relaxation rate was measured for the first time in experiments reported in [10] in order to study the dependence of the cluster degradation rate on the coherence order. Thus, according to Eq. (7),

$$\frac{G_M(T,t_1=0)}{G_M(T,t_1=\tau)} = e$$
$$= \exp\left(2\sqrt{qM^2} - 2\sqrt{q_0M^2} + A^2M^2\tau^2\right) \quad (11)$$
$$\times\frac{1+2\sqrt{q_0M^2}}{1+2\sqrt{qM^2}}\left(\frac{q}{q_0}\right)^{3/2},$$

where $q_0 = 2/\bar{K}_0$. To solve Eq. (11), it is expedient to pass to new variables that "scale" the coordinate axes:

$$m^2 = q_0M^2 = 2M^2/\bar{K}_0;$$
$$z = \sqrt{q/q_0} = \left(1+\bar{K}_0B^2\tau^2/4\right)^{1/2}. \quad (12)$$

In new variables $A^2M^2\tau^2 = 2\alpha m^2(z^2-1)$ (where $\alpha = A^2/B^2$), Eq. (11) takes the form at $m \geq 0$

$$\exp\left\{2m(z-1) + 2\alpha m^2(z^2-1)\right\}\frac{1+2m}{1+2mz}z^3 = e. \quad (13)$$

Approximate solutions of Eq. (13) for large and small m values can be found analytically. At $m^2 \ll 1$, we find

$$R(m) = \frac{1}{\sqrt{\bar{K}_0}B\tau} = \frac{1}{2\sqrt{z^2-1}}$$
$$\approx \frac{1}{2\sqrt{e^{2/3}-1}}\left[1+m^2(1+\alpha)\frac{2}{3}e^{2/3}\right] \quad (14)$$
$$= 0.5136\left[1+1.298m^2(1+\alpha)\right].$$

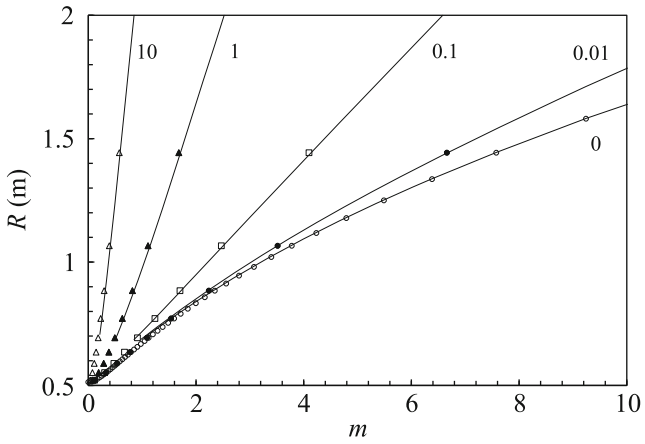

Fig. 1. Scaled relaxation (decoherence) rate of the component of the multiple-quantum spectrum $R(m) = \frac{1}{\sqrt{\bar{K}_0}B\tau}$ versus the scaled coherence order $m = \sqrt{2M^2/\bar{K}_0}$ at different parameters $\alpha = A^2/B^2$ indicated by numbers near the lines according to (lines) approximate formula (15) and (symbols) the numerical solution of Eq. (13).

If $m^2 \gg 1$, the solution of Eq. (13) has the form

$$R(m) \approx \frac{1}{2\sqrt{2\delta_0}}\left(1 + \frac{1}{2m(1+2\alpha m)} - \frac{\delta_0}{4}\right), \qquad (15)$$

$$\delta_0 = \frac{1/m}{1 + 2\alpha m + \sqrt{(1+2\alpha m)^2 + 2\alpha}}, \qquad (16)$$

where δ_0 is the solution providing the equality of the exponent in Eq. (13) to 1. In particular, at $m^2 \gg 1$ and $\alpha = 0$,

$$R(m) = \frac{1}{\sqrt{\bar{K}_0}B\tau} = \frac{\sqrt{m}}{2}\left(1 + \frac{3}{8m}\right), \qquad (17)$$

and at $m^2 \gg 1$ and $m\alpha \gg 1$,

$$R(m) \approx \frac{\sqrt{\alpha}m}{\sqrt{2}} \approx \left(1 + \frac{1}{4\alpha m} + \frac{1}{16\alpha m^2}\left(1 + \frac{2.5}{\alpha}\right)\right). \qquad (18)$$

The numerically found solution of Eq. (13) for different α values is shown in Fig. 1 in scaled coordinates:

$$R(m) = \frac{1}{\sqrt{\bar{K}_0}B\tau}, \quad \text{where} \quad m = \sqrt{2M^2/\bar{K}_0}. \qquad (19)$$

The approximate dependences shown in Fig. 1 and those calculated by Eq. (15) describe well the results of exact calculations at large m. The appearance of an additional contribution to the spin relaxation of clusters arising from the action of a "correlated field" (i.e., at $A \neq 0$) leads to the acceleration of the growth rate of R as a function of M.

The dependences obtained for the relaxation rates R of the components of the multiple-quantum spectrum on the coherence order M demonstrate the transition from the quadratic dependence $R(m) \sim M^2$ in Eq. (14) to the square root one $R(m) \sim \sqrt{M}$ in Eq. (17) with increasing M. A similar slowdown in the growth of the relaxation rate was observed experimentally (see Fig. 5 in [10]). To explain this effect, a formula with the sum of two contributions to relaxation was proposed in [17]. For a more thorough comparison of our proposed theory with experiment, the data (part of them at $M \geq 0$) given in Fig. 5 in [10] were digitized and rebuilt in Fig. 2 in coordinates scaled by $\sqrt{\bar{K}}$. The vertical axis shows the experimental relaxation rates divided by $\sqrt{\bar{K}}$, and the horizontal axis shows $m_g = \sqrt{2M^2/\bar{K}}$. We note that the proportionality of the relaxation rate to the quantity $\sqrt{\bar{K}}$ was found experimentally in [10]. From the same work, we took the $\bar{K}$ values at different durations T, which were calculated in terms of the FWHMs of multiple-quantum spectra σ. The authors assumed that the spectrum had a Gaussian shape given by Eq. (3), and, consequently,

$$\bar{K} = \bar{K}_{0g} = \frac{1}{\ln 2}\left(\frac{\sigma}{2}\right)^2. \qquad (20)$$

However, Eq. (9) for the shape of the spectrum implies a different relation between $\bar{K} = \bar{K}_0$ and this width:

$$\bar{K} = \bar{K}_0 = 2\left(\frac{2}{x}\right)^2\left(\frac{\sigma}{2}\right)^2. \qquad (21)$$

Here, $x \approx 1.68$ is the solution of the equation $e^x = 2(1+x)$. Thus, we arrive at the relation

$$\bar{K}_{0g}/\bar{K}_0 \approx 0.509 = (0.7134)^2. \qquad (22)$$

In addition to the experimental dependences, Fig. 2 shows the theoretical dependences of the relaxation rate of coherent states obtained by numerically solving Eq. (13) for $\alpha =$ (dotted line) 0, (dashed line) 0.1, and (solid line) 0.5. Taking into account Eq. (22) and the parameter $B = 9.27 \times 10^{-3}$ μs^{-1} taken from the experiment, these dependences are represented by the function $R(0.7134m_g)$ 13/ms. Let us explain its form: first, the theoretical velocity $R(m)$ (Fig. 1) is a function of $m = \sqrt{2M^2/\bar{K}_0}$, while the experimental velocity in Fig. 2 is a function of $m_g = \sqrt{2M^2/\bar{K}_{0g}}$. The ratio of arguments is $m = \sqrt{\bar{K}_{0g}/\bar{K}_0}m_g = 0.7134m_g$. Second, we want the theoretical relaxation rate (14) $R(0) = \frac{1}{\sqrt{\bar{K}_0}B\tau} = 0.5136$ to coincide with the experimental

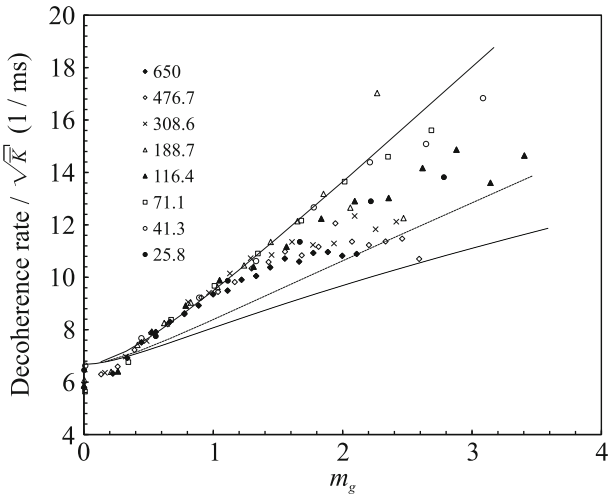

Fig. 2. Experimental relaxation (decoherence) rate [10] divided by $\sqrt{\bar{K}}$ versus the coherence order M taken in the form $m_g = \sqrt{2M^2/\bar{K}}$. Results obtained at different average cluster sizes $\bar{K} = \bar{K}_{0g}$ (column of numbers in the figure) are shown by different symbols. Theoretical results found by the numerical solution of Eq. (13) are shown by lines as functions $13R(0.7134m_g)$/ms at the parameters α = (dotted line) 0, (dashed line) 0.1, and (solid line) 0.5.

$\frac{1}{\tau\sqrt{\bar{K}_{0g}}} \approx 6.68\ \frac{1}{\text{ms}}$ at $M = 0$. From here, we find the values of the coefficient $13\ \frac{1}{\text{ms}} \approx \frac{B\sqrt{\bar{K}_0}}{\sqrt{\bar{K}_0 g}}$ and parameter $B \approx 0.7134 \times 13\ \text{ms}^{-1} = 9.2742\ \text{ms}^{-1}$.

When scaling the data in Fig. 2, we used Eq. (7). Previously, data scaling in multiple-quantum spectroscopy was performed in [15, 26, 27]. In [26], each multiple-quantum spectrum obtained by increasing the preparation time was scaled by its width (albeit with some reservations). The authors of [15, 27] studied the effect of a perturbation added during the preparatory period and performed scaling of the growth of the average cluster size [27] and the damping of the total intensity of the multiple-quantum spectrum [15]. For scaling, power functions are taken with selected exponents.

It can be seen in Fig. 2 that the dependence with $\alpha = 0.5$ somewhat better agrees with the experimental results [10] than for the other α values we used. However, good agreement with experiment is observed in the range of m values on the order of unity, while the theoretical dependence on m at large m is stronger than the experimental one. Apparently, this indicates that the representation of the contribution to degradation from the correlated field in Eq. (1) by the Gaussian function on M is inaccurate for large M values, i.e., for large clusters. The topology of clusters should be taken into account, which leads to the replacement of one relaxation function by the sum of functions depending on the cluster size and the ratio of its surface to the volume [28]. A non-Gaussian dependence of the relaxation rate on M was considered in, e.g., [29], where the relaxation of the multiple-quantum spectrum components for a system with a large number of equivalent spins was numerically calculated. Since the dipole–dipole coupling constants between all spins are the same, only the correlated contribution to the local field remains. The authors of [29] show that the relaxation time decreases with an increase in the number of spins and the order of multiple-quantum coherence M. In this case, the rate of change decreases at large M values.

Thus, the physical model developed in this work has made it possible for the first time to take into account the size distribution of clusters of dynamically correlated spins and to study their degradation under the action of a perturbation. Previously, we analyzed the dependence of the relaxation rate on the coherence order M in the model of a single cluster with a certain average size [19]. In particular, we found the value $A^2 = 205\ \text{ms}^{-2}$ (at $T = 660\ \mu\text{s}$) for the magnitude of the correlated contribution, which is solely responsible for the dependence on M in this approach. In this work, we have calculated the contribution of the uncorrelated field from Eq. (1) to the dependence of the relaxation rate on the quantity M taking into account the size distribution of clusters given by Eq. (2). The separation of this contribution reduces the contribution of the second factor in Eq. (1) to the value $A^2 \approx 43\ \text{ms}^{-2}$. Thus, the hypothesis of the authors of [10] about a possible connection between the observed dependence of the relaxation rate on order M and the presence of clusters of different sizes is confirmed. Finally, we have shown that a comparison of the proposed theory with experiment allows the "numerical" separation of the correlated and uncorrelated contributions to the local field on the nuclei of a multispin cluster and to the decoherence rate.

ACKNOWLEDGMENTS

We are grateful to K.V. Zobov for his help in digitizing the experimental curves from [10] and numerically solving Eq. (13).

FUNDING

This work was supported by the Ministry of Science and Higher Education of the Russian Federation (state assignment no. 122040500060-4).

CONFLICT OF INTEREST

The authors declare that they have no conflicts of interest.

REFERENCES

1. P. Gaspard, in *Proceedings of the Symposium Henri Poincare,* Ed. by P. Gaspard, M. Henneaux, and F. Lambert (Int. Solvay Inst. Phys. Chem., Brussels, 2007), p. 97.
2. D. Preskill, *Quantum Information and Quantum Computing* (Regulyar. Khaot. Dinamika, Moscow, 2008), Vol. 1 [in Russian].
3. D. Suter and G. A. Álvarez, Rev. Mod. Phys. **88**, 041001 (2016).
4. L. Pezze, A. Smerzi, M. K. Oberthaler, R. Schmied, and P. Treutlein, Rev. Mod. Phys. **90**, 035005 (2018).
5. J. Preskill, Quantum **2**, 79 (2018).
6. Bin Cheng, Xiu-Hao Deng, Xiu Gu, Yu He, et al., arXiv: 2303.04061 (2023).
7. T. Kusumoto, K. Mitarai, K. Fujii, M. Kitagawa, and M. Negoro, npj Quantum Inf. **7**, 94 (2021).
8. J. Baum, M. Munovitz, A. N. Garroway, and A. Pines, J. Chem. Phys. **83**, 2015 (1985).
9. R. Ernst, G. Bodenhausen, and A. Wokaun, *Principles of NMR in One and Two Dimensions* (Clarendon, Oxford, 1987).
10. H. G. Krojanski and D. Suter, Phys. Rev. Lett. **93**, 090501 (2004).
11. H. G. Krojanski and D. Suter, Phys. Rev. A **74**, 062319 (2006).
12. G. Cho, P. Cappelaro, D. G. Cory, and C. Ramanathan, Phys. Rev. B **74**, 224434 (2006).
13. C. M. Sanchez, R. H. Acosta, P. R. Levstein, H. M. Pastawski, and A. K. Chattah, Phys. Rev. A **90**, 042122 (2014).
14. G. A. Álvarez and D. Suter, Phys. Rev. A **84**, 012320 (2011).
15. F. D. Domínguez, M. C. Rodríguez, R. Kaiser, D. Suter, and G. A. Alvarez, Phys. Rev. A **104**, 012402 (2021).
16. C. M. Sanchez, A. K. Chattah, and H. M. Pastawski, Phys. Rev. A **105**, 052232 (2022).
17. A. Fedorov and L. Fedichkin, J. Phys.: Condens. Matter **18**, 3217 (2006).
18. A. A. Lundin and B. N. Provotorov, Sov. Phys. JETP **43**, 1149 (1976).
19. V. E. Zobov and A. A. Lundin, J. Exp. Theor. Phys. **112**, 451 (2011).
20. V. E. Zobov and A. A. Lundin, J. Exp. Theor. Phys. **103**, 904 (2006).
21. V. E. Zobov and A. A. Lundin, Russ. J. Phys. Chem. B **27**, 676 (2008).
22. A. A. Lundin and V. E. Zobov, J. Exp. Theor. Phys. **120**, 762 (2015).
23. V. E. Zobov and A. A. Lundin, Appl. Magn. Res. **52**, 879 (2021).
24. V. E. Zobov and A. A. Lundin, J. Exp. Theor. Phys. **135**, 752 (2022).
25. A. P. Prudnikov, Yu. A. Brychkov, and O. I. Marichev, *Integrals and Series* (Nauka, Moscow, 1981; Gordon and Breach, New York, 1986), Vol. 1, Sect. 2.3.16(2).
26. S. Lacelle, S. Hwang, and B. Gerstein, J. Chem. Phys. **99**, 8407 (1993).
27. G. A. Alvarez, D. Suter, and R. Kaiser, Science (Washington, DC, U. S.) **349**, 846 (2015).
28. V. E. Zobov, Theor. Math. Phys. **165**, 1443 (2010).
29. S. I. Doronin, E. B. Fel'dman, and A. I. Zenchuk, J. Chem. Phys. **134**, 034102 (2011).

Translated by L. Mosina